

Microscopic theory of quadrupolar ordering in TmTe

A.V. Nikolaev* and K.H. Michel
*Department of Physics, University of Antwerp, UIA,
2610 Antwerpen, Belgium
(November 11, 2018)*

We have calculated the crystal electric field of TmTe ($T > T_Q$) and have obtained that the ground state of a Tm $4f$ hole is the Γ_7 doublet in agreement with Mössbauer experiments. We study the quadrupole interactions arising from quantum transitions of $4f$ holes of Tm. An effective attraction is found at the L point of the Brillouin zone, \bar{q}_L . Assuming that the quadrupolar condensation involves a single arm of \bar{q}_L we show that there are two variants for quadrupole ordering which are described by the space groups $C2/c$ and $C2/m$. The Landau free energy is derived in mean-field theory. The phase transition is of second order. The corresponding quadrupole order parameters are combinations of T_{2g} and E_g components. The obtained domain structure is in agreement with observations from neutron diffraction studies for TmTe. Calculated lattice distortions are found to be different for the two variants of quadrupole ordering. We suggest to measure lattice displacements in order to discriminate between those two structures.

I. INTRODUCTION

The monochalcogenides of rare-earth elements crystallizing in the rocksalt structure, exhibit interesting electrical, optical and magnetic properties.¹ In TmTe thulium is in a divalent state with one $4f$ -hole ($4f^{13}$) localized at each Tm site. At room temperature TmTe is a semiconductor with the electron band energy gap 0.25 eV (from photoemission data) and an $f \rightarrow d$ band gap 0.35 eV (from absorption data)². Magnetic structure determination leads to a type II antiferromagnet below the Néel temperature³ $T_N = 0.43$ K. Under pressure of 2 GPa TmTe undergoes a semiconductor-metal transition⁴ where a ferromagnetic order occurs⁵ with a Curie temperature $T_C = 14$ K for 2.7 GPa. At pressure of 5.7 GPa TmTe undergoes a structural phase transition to a tetragonal structure^{6,7} with a further decrease of resistivity.⁴ A renewed interest to TmTe has emerged from the recent unexpected discovery of an antiferroquadrupolar (AFQ) phase transition below $T_Q = 1.8$ K at atmospheric pressure.⁸ The transition was first revealed by specific heat measurements⁸ and then confirmed by elastic constant anomalies⁹ and by neutron diffraction in an external magnetic field.¹⁰ In the quadrupolar ordered state by the application of a uniform magnetic field superlattice neutron Bragg peaks, corresponding to the wave vector $\vec{q} = (2\pi/a)(1/2, 1/2, 1/2)$, appear in addition to the normal ferromagnetic intensity superimposed on the nuclear peaks¹⁰ (see for a review Ref. 11 and for recent development Refs. 12,13). Thus TmTe has been found to belong to an increasing family of rare-earths¹⁴ (TmCd, TmAu₂, CeB₆, DyB₂C₂ and so on) which exhibit quadrupolar ordering.

An important insight in the nature of the AFQ ordering of TmTe can be gained on the basis of a classical description of multipoles presented in Refs. 15,16. However, the theoretical treatment in Refs. 15,16 is based on

a phenomenological Hamiltonian where the quadrupole-quadrupole interactions are taken to be isotropic in the subspaces of Γ_3 (E_g) and Γ_5 (T_{2g}) irreducible representations of the cubic point group O_h . In addition, a coupling between these representations is neglected. Such a treatment has shortcomings and does not allow to determine the crystal structure. Indeed, since the quadrupolar interaction forces are of short range, it is necessary to take into account the structure of the face centered cubic (fcc) lattice and the full matrix character of the quadrupolar interactions. Furthermore, the coupling of T_{2g} and E_g representations is important and affects the quadrupolar phase transition. It is the purpose of the present paper to investigate the quadrupolar phase transition and to determine the crystal structure (space group) of the quadrupolar ordered phase. Hence it is necessary that the symmetries of quadrupolar interactions on a fcc lattice are carefully taken into account. Multipolar interactions of E_g and T_{2g} modes on a fcc lattice have been studied earlier in connections with the problem of orientational order in a molecular crystal, solid C₆₀.¹⁷

In constructing a microscopic theory of quadrupolar ordering in TmTe we will use the concepts we have developed recently^{18,19} for the description of the $\gamma - \alpha$ transition in Ce. We will take advantage of the fact that Tm and Ce are mirror elements in the series of lanthanides. We recall that Ce has one single electron in the $4f$ shell while Tm has one hole (electron configuration $4f^{13}$). While Ce is a metal, TmTe is an insulator for T near T_Q . Hence we will neglect the polarization of conduction electrons (which contributes to the quadrupolar interaction¹⁹ in Ce) in our treatment of TmTe. Because of charge transfer from Tm to Te, only a small fraction of conduction electron density is left around the Tm⁺⁺ ion.

In zero magnetic field the magnetic susceptibility of TmTe shows a small anomaly at T_Q .⁹ Thus the

quadrupolar ordering is not directly connected⁹ with the magnetic ordering in TmTe which occurs at still lower temperature T_N . Therefore in this paper we limit ourselves to the charge degrees of freedom leaving the magnetic properties for future considerations.

The content of the present paper is the following. In Section II we calculate the crystal field which refers to the $4f$ hole in TmTe. The result is compared with experimental data. Next (Sect. III) we study the quadrupolar interactions and the resulting phase transition. We suggest condensation schemes leading to the monoclinic space groups $C2/c$ or $C2/m$. In order to discriminate between these space groups, we calculate the accompanying lattice distortions (Sect. IV) and suggest synchrotron radiation experiments. Finally, the results of our work are summarized and commented in the Conclusions (V).

II. CRYSTAL FIELD

The issue of the crystal electric field (CEF) of TmTe is controversial. A Schottky specific heat peak around 5 K has been found indicating that the total CEF splitting is about 15 K.²⁰ From thermal expansion data at low temperature (2-16 K) the following sequence $\Gamma_8(0 \text{ K}) - \Gamma_7(10 \text{ K}) - \Gamma_6(16 \text{ K})$ has been proposed.²¹ Recent inelastic neutron scattering experiment supports the Γ_8 ground state.²² However, from Mössbauer spectroscopy another scheme, $\Gamma_7(0 \text{ K}) - \Gamma_8(12 \text{ K}) - \Gamma_6(19.6 \text{ K})$, has been deduced.²³ The latter sequence was also obtained by detailed ultrasonic velocity measurements.²⁴ Here we would like to remark that some of these results are not direct and depend on conditions, methods and models used to fit experimental data.

As a starting point of our derivation of the CEF we recall that here we consider the effect on the hole in the $4f$ shell of Tm^{++} . In comparison with the case of one electron (as in Ce), the position of the corresponding energy levels is reversed. For ions of lanthanides in solids the spin-orbit coupling

$$V_{so} = \zeta \vec{L} \cdot \vec{S} \quad (2.1)$$

dominates crystal field effects. The potential V_{so} has spherical symmetry. Here \vec{L} and \vec{S} are the orbital and the spin angular momentum operators, $\vec{J} = \vec{L} + \vec{S}$ is the total angular momentum, with eigenvalues of J_z : $J = 7/2$ and $J = 5/2$. In Eq. (2.1) ζ is the spin-orbit coupling constant. In case of a hole, the lower energy level corresponds to the state $D_{7/2}$ (degeneracy 8) and the higher level to $D_{5/2}$ (degeneracy 6). The experimental energy separation² $\Delta_{so} = -(7/2)\zeta$ is given by 1.24 eV, corresponding to $\zeta = -4112 \text{ K}$. In presence of the cubic crystal field V_{CF} , the hole experiences the potential

$$V_0^f = V_{so} + V_{CF}. \quad (2.2)$$

Since V_{CF} has cubic symmetry, the degeneracies of the spin-orbit levels are lifted according to the scheme²⁵

TABLE I. Angular-momentum-decomposed electronic charges Q_i^A and total charges Q^A inside Tm and Te MT spheres and in the interstitial region (LAPW calculations, see Ref. 31 for details and definitions).

A	Tm	Te	interstices
Q_s^A	0.161e	1.827e	—
Q_p^A	0.140e	4.084e	—
Q_d^A	0.275e	0.013e	—
Q^A	+1.509 e	+0.079 e	-1.588 e

$$D_{\frac{5}{2}} \rightarrow \Gamma_7 + \Gamma_8, \quad (2.3a)$$

$$D_{\frac{7}{2}} \rightarrow \Gamma_6 + \Gamma_7 + \Gamma_8, \quad (2.3b)$$

where $\Gamma_6, \Gamma_7, \Gamma_8$ are irreducible representations of the double cubic group O_h' .

Usually for CEF calculations²⁵ the lowest J multiplet is used and the CEF $4f$ Hamiltonian is expressed in terms of Stevens equivalent operators J_x, J_y and J_z .^{26,25} A thorough discussion on microscopic origin of the crystal field effects is given by Newman.^{27,28} Here we will follow the method of Refs. 18,19 which allows us to calculate CEF using results of electron band structure calculations as a starting point. Our approach is not restricted to the J multiplet with lowest energy. Since we may neglect conduction electrons (see Sect. I), the problem of the CEF of one $4f$ hole then becomes similar to the CEF of one $4f$ electron considered in Ref. 18 with the only difference that in the following we take into account the radial dependence of the $4f$ hole in TmTe. Our goal is then to diagonalize the potential V_0^f and to determine the associated 14 eigenvalues ε_i .

In order to proceed, we first need to know the charge distribution in the TmTe unit cell. The previous electron band structure calculation²⁹ of TmTe in the local density approximation (LDA) does not give such information. We then have performed our linear augmented plane wave (LAPW) calculations using LDA and the muffin-tin (MT) approximation.³⁰ The MT radii 2.9 and 3.1036 a.u. were chosen for Tm and Te, respectively. The MT potential and density of Tm and Te have been obtained self-consistently using a LAPW basis of ~ 170 plane wave functions on a 20-point mesh of the irreducible domain of the fcc Brillouin zone. During the calculations the f electrons of Tm were treated as core states with an occupation number of 13 but were allowed to adjust self-consistently to the conduction electron density. We did tabulate the radial dependence \mathcal{R}_f of the $J = 7/2$ electronic $4f$ states of Tm on a set of 70 points with $0.111 \leq r \leq 2.971 \text{ a.u.}$ Notice that \mathcal{R}_f is obtained as an output of the electronic band structure calculation of TmTe and thereby deviates from the $4f$ electronic density of a Tm atom. The results of the charge density calculations are quoted in Table I. Using the MT potential, we have calculated the spin-orbit splitting. The $D_{5/2}$ states of the $4f$ hole of Tm were found to be separated from the $D_{7/2}$ states by $\Delta'_{so} = 1.21 \text{ eV}$, which is close

to the experimental value of Ref. 2. In the following we consider expression (2.1) of V_{so} with $\zeta = -4112$ K.

In constructing the crystal field operator V_{CF} , we restrict ourselves to the effect of the six nearest Te neighbors in octahedral position around a Tm^{++} ion at site \vec{n} . (Later we will discuss the limitation of the present approach.) Since the crystal field has cubic symmetry, we write it in form of a multipole expansion, following the method of Ref. 18, Appendix A:

$$V_{CF}(\vec{n}) = B_4^f \rho_{\Lambda_1}^F(\vec{n}) + B_6^f \rho_{\Lambda_2}^F(\vec{n}). \quad (2.4)$$

Here $\rho_{\Lambda_1}^F, \rho_{\Lambda_2}^F$ are the hole charge density operators, $\Lambda_1 \equiv (l = 4, A_{1g})$ refers to the lowest (non-trivial) multipole ($l = 4$) of symmetry A_{1g} (unit representation of O_h), while $\Lambda_2 \equiv (l = 6, A_{1g})$ corresponds to the next with $l = 6$. Explicitly, we have ($p = 1, 2$):

$$\rho_{\Lambda_p}^F(\vec{n}) = \sum_{ij} c_{\Lambda_p}^f(ij) |i\rangle_{\vec{n}} \langle j|_{\vec{n}}, \quad (2.5)$$

where the basis states $|i\rangle$ are $4f$ states, and where

$$c_{\Lambda_1}^F(ij) = \langle i | S_{l=4}^{A_{1g}} | j \rangle, \quad (2.6a)$$

$$c_{\Lambda_2}^F(ij) = \langle i | S_{l=6}^{A_{1g}} | j \rangle, \quad (2.6b)$$

$S_{\Lambda_1} \equiv S_4^{A_{1g}}$ and $S_{\Lambda_2} \equiv S_6^{A_{1g}}$ being the site symmetry adapted functions³² (SAF). The function $S_4^{A_{1g}}$ is given explicitly by Eq. (A.8) of Ref. 18, the function $S_6^{A_{1g}}$ is

$$S_6^{A_{1g}}(\Theta, \phi) = \sqrt{\frac{1}{8}} Y_6^0(\Theta, \phi) - \sqrt{\frac{7}{8}} Y_6^{4,c}(\Theta, \phi). \quad (2.7)$$

The superscript F stands for quantum transitions between $4f$ states of the hole. Taking as basis states the functions of the irreducible representations T_{1u}, T_{2u} and A_{2u} of O_h , we obtain the diagonal coefficients $c_{\Lambda_1}^F(A_{2u}) = -0.23505$, $c_{\Lambda_1}^F(T_{2u}) = -0.03917$, $c_{\Lambda_1}^F(T_{1u}) = 0.11752$ for Λ_1 and $c_{\Lambda_2}^F(A_{2u}) = 0.20118$, $c_{\Lambda_2}^F(T_{2u}) = -0.15088$, $c_{\Lambda_2}^F(T_{1u}) = 0.08382$ for Λ_2 . Notice that there is no term with $l = 8$ in the expansion series (2.4).²⁵ Although in principle one can consider the function³² $S_{l=8}^{A_{1g}}$, the corresponding matrix elements $\langle i | S_{l=8}^{A_{1g}} | j \rangle$ vanish for $4f$ orbitals. The coefficients B_4^f and B_6^f are given by

$$B_4^f = \frac{6}{\sqrt{4\pi}} Q_{eff} e_h v_{\Lambda_1 0}^F, \quad (2.8a)$$

$$B_6^f = \frac{6}{\sqrt{4\pi}} Q_{eff} e_h v_{\Lambda_2 0}^F. \quad (2.8b)$$

Here e_h refers to the charge of the hole, Q_{eff} to the effective charge of Te and $v_{\Lambda_p 0}^F$ is given by the radial average of the Λ_p -th multipole of the Coulomb potential:

$$v_{\Lambda_p 0}^F = \int dr r^2 \mathcal{R}_f^2(r) v_{\Lambda_p 0}(\vec{n}, \vec{n}'; r, r'), \quad (2.9a)$$

TABLE II. Calculated CEF spectrum of a $4f$ hole in the disordered phase ($T > T_Q$), $\Delta\varepsilon=14389.4$ K.

i		ε_i
1, 2	$\Gamma_7, 1$	0 K
3 - 6	$\Gamma_8, 1$	5.81 K
7, 8	Γ_6	9.65 K
9, 10	$\Gamma_7, 2$	$\Delta\varepsilon$
11 - 14	$\Gamma_8, 2$	$\Delta\varepsilon+6.60$ K

where \mathcal{R}_f is the radial function¹⁹ and

$$v_{\Lambda_p 0}(\vec{n}, \vec{n}'; r, r') = \frac{1}{\sqrt{4\pi}} \int d\Omega(\vec{n}) d\Omega(\vec{n}') \frac{S_{\Lambda_p}(\Omega(\vec{n}))}{|\vec{R}(\vec{n}) - \vec{R}'(\vec{n}')|}. \quad (2.9b)$$

In the last integrals we have $\vec{R}(\vec{n}) = \vec{X}(\vec{n}) + \vec{r}(\vec{n})$ where $\vec{X}(\vec{n})$ is the lattice site position and $\vec{r}(\vec{n})$ the hole (electron) radius vector, $\vec{r} = (r, \vec{\Omega})$, $\vec{\Omega} = (\Theta, \phi)$.

We take $Q_{eff} = Q^{Te}$, Table I. In Eqs. (2.9a,b) \vec{n} refers to a Tm lattice site, while \vec{n}' - to any of its six Te neighbors. Diagonalization of $V_{CF}(\vec{n})$ leads to the crystal field term scheme without spin-orbit coupling:

$$\varepsilon(\Gamma) = B_4^f c_{\Lambda_1}^F(\Gamma) + B_6^f c_{\Lambda_2}^F(\Gamma), \quad (2.10)$$

where $\Gamma = A_{2u}, T_{2u}$ and T_{1u} . Our calculations yield $B_4^f=35.73$ K, $B_6^f=1.631$ K and $\varepsilon(A_{2u}) = -8.07$ K, $\varepsilon(T_{2u}) = -1.646$ K, $\varepsilon(T_{1u}) = 4.336$ K. Including next the spin-orbit coupling and proceeding as in appendix A of Ref. 18, we obtain the CEF term spectrum ε_i of the $4f$ hole, quoted in Table II.

If one goes beyond the present nearest neighbor approximation, the calculation becomes much more complex. Considering the charge contributions from the twelve neighboring Tm sites and $Q^{int} = -1.588|e|$ from the interstitial region, we find that the crystal field splittings between energy levels increase by roughly an order of magnitude in comparison with the values of Table II, $\varepsilon(\Gamma_8, 1) - \varepsilon(\Gamma_7, 1)=62.9$ K, $\varepsilon(\Gamma_6) - \varepsilon(\Gamma_7, 1)=102.5$ K. The increase is mainly caused by a larger positive value of Q_{eff} in Eqs. (2.8a,b) when the homogeneous electron charge distribution in the interstitial region is taken into account.³³ Notice, however, that the sequence $\Gamma_7 - \Gamma_8 - \Gamma_6$ with Γ_7 as a ground state is conserved. The other remote shells of neighbors have been found to produce little changes on the calculation since the corresponding integrals vary like³⁴ $|\vec{R}(\vec{n}) - \vec{R}(\vec{n}')|^{-5}$ for $S_{\Lambda_1}^{A_{1g}}$ and $|\vec{R}(\vec{n}) - \vec{R}(\vec{n}')|^{-7}$ for $S_{\Lambda_2}^{A_{1g}}$. The magnitude of the CEF splittings in the latter approach is reduced by several effects: screening due to polarization of conduction electrons,¹⁹ which are still present on each Tm site (see Table I), and an inhomogeneous charge distribution in the interstitial volume. The first effect is due to the coupling of $4f$ localized electrons with $5d$ conduction electron states which was discussed by Newman.²⁸ In our

model the interactions with the conduction electrons are given by Eq. (4.10) of Ref. 19. However, such calculation would require a self-consistent procedure¹⁹ for $4f$ and conduction electrons included in an electron band structure scheme and is beyond the scope of the present work which is focused on quadrupolar ordering. Some authors^{35,27} have emphasized the role of covalent mixing which involves one-electron matrix elements between the $4f$ electrons with $5d$ electrons on other atoms. Notice that such effects imply nonorthogonal basis functions on neighboring sites. In LAPW³¹ and linear muffin-tin orbital (LMTO)³⁶ methods of electron band structure calculations there is no overlap between MT basis functions belonging to different sites, while $4f$ electronic wave functions are confined inside MT spheres. The covalent effect which is associated with anisotropic character of chemical bonding then may be described by inhomogeneity of electron charge distribution in the interstitial region and inside MT spheres. Since there is a large portion of electronic charge situated in the interstices (Q^{int}) it is likely that the effect of the charge inhomogeneity is appreciable.

In summary we here obtain the sequence $\Gamma_7 - \Gamma_8 - \Gamma_6$ with Γ_7 as ground state, in agreement with results from Mössbauer spectroscopy²³ and ultrasonic velocity measurements.²⁴ Although the present calculation of CEF is incomplete our estimations show that the sequence is likely to be conserved in a full treatment of the problem. The experimental identification of the ground state as Γ_8 is in contradiction with the present calculations. The discrepancy can arise due to strong fluctuations of quadrupole density which occurs at temperature $T \sim 2 - 3$ K and affect the experimental results. Indeed, the presence of quadrupolar fluctuations have been found at 3 K in Mössbauer studies of TmTe.²³ It is necessary to analyze both the experimental conditions and methods of obtaining the CEF levels and of identifying the states. Further investigations and full calculations of CEF are needed in order to clarify the issue. On the other hand, we want to stress that theoretically a quadrupole order can occur even if the ground state of the $4f$ hole is Γ_7 (or Γ_6)^{18,24} while Γ_8 remains an excited state.

III. PHASE TRANSITION

Here we will discuss the antiferroquadrupolar phase transition in TmTe. In fact this phase transition is a structural one, with the concomitant symmetry change cubic \rightarrow monoclinic. In the following we will continue to exploit the duality electron-hole between Ce and TmTe. In Ref. 18 we have shown that the Coulomb interaction operator between $4f$ electrons (holes) on a fcc lattice is obtained as a double multipole expansion

$$U^{ff} = \frac{1}{2} \sum'_{\vec{n}\vec{n}'} \sum_{\Lambda\Lambda'} \rho_{\Lambda}^F(\vec{n}) v_{\Lambda\Lambda'}(\vec{n} - \vec{n}') \rho_{\Lambda'}^F(\vec{n}'). \quad (3.1)$$

Here the expansion coefficients $v_{\Lambda\Lambda'}$ are given by

$$v_{\Lambda\Lambda'}(\vec{n} - \vec{n}') = \int dr r^2 \int dr' r'^2 \times \mathcal{R}_f^2(r) \mathcal{R}_f^2(r') v_{\Lambda\Lambda'}(\vec{n}, \vec{n}'; r, r'), \quad (3.2a)$$

where

$$v_{\Lambda\Lambda'}(\vec{n} - \vec{n}'; r, r') = \int d\Omega(\vec{n}) d\Omega(\vec{n}') \frac{S_{\Lambda}(\hat{n}) S_{\Lambda'}(\hat{n}')}{|\vec{R}(\vec{n}) - \vec{R}'(\vec{n}')|}. \quad (3.2b)$$

For details on the radial average in Eq. (3.2a), see Ref. 19. Here $S_{\Lambda}(\hat{n})$, $\hat{n} \equiv (\Theta(\vec{n}), \phi(\vec{n}))$, are site symmetry adapted functions³², Λ stands for (l, τ) , where l accounts for the angular dependence of the multipolar expansion and $\tau = (\Gamma, k)$, Γ denoting the irreducible representation of the site point group and k labeling the rows of Γ . In our case, $l = 2$ (quadrupoles) and Γ stands for the representations T_{2g} ($k = 1 - 3$) and E_g ($k = 1, 2$) of the cubic site group O_h . The corresponding SAFs $S_{T_{2g}}^k$ and $S_{E_g}^k$ are given by Eqs. (2.16) and (2.15) of Ref. 18. The quantity $\rho_{\Lambda}^F(\vec{n})$ stands for the multipolar density

$$\rho_{\Lambda}^F(\vec{n}) = \sum_{ij} c_{\Lambda}^F(ij) |i\rangle_{\vec{n}} \langle j|_{\vec{n}}, \quad (3.3)$$

with

$$c_{\Lambda}^F(ij) = \int d\Omega |i\rangle_{\hat{n}} S_{\Lambda}(\hat{n}) \langle j|_{\hat{n}}. \quad (3.4)$$

Introducing Fourier transforms

$$\rho_{\Lambda}^F(\vec{q}) = \frac{1}{\sqrt{N}} \sum_{\vec{n}} e^{i\vec{q}\cdot\vec{X}(\vec{n})} \rho_{\Lambda}^F(\vec{n}), \quad (3.5a)$$

$$v_{\Lambda\Lambda'}(\vec{q}) = \sum'_{\vec{h}\neq 0} e^{i\vec{q}\cdot\vec{X}(\vec{h})} v_{\Lambda\Lambda'}(\vec{h}), \quad (3.5b)$$

where \vec{q} is the wave vector, we get for the quadrupole-quadrupole interaction

$$U_{QQ}^{ff} = \frac{1}{2} \sum_{\vec{q}} \sum_{\Lambda\Lambda'} \rho_{\Lambda}^F(\vec{q})^\dagger v_{\Lambda\Lambda'}(\vec{q}) \rho_{\Lambda'}^F(\vec{q}). \quad (3.6)$$

The 5×5 matrix $v_{\Lambda\Lambda'}$ is given by the expressions (A1, A6) and (A7) of Ref. 17. This matrix has negative eigenvalues at some points of the Brillouin zone (BZ). The largest negative eigenvalues have been found at the X and L points of the BZ. Since the superstructure reflections have been found by neutron-diffraction experiments¹⁰ on TmTe at the L point of the BZ, $\vec{q}_L = (2\pi/a)(1/2, 1/2, 1/2)$, we limit in the following our considerations to the L point.

There are four arms of the star $^*\vec{q}_L$ which we label by $\vec{q}_L^1 = (1/2, 1/2, 1/2)$, $\vec{q}_L^2 = (-1/2, 1/2, 1/2)$, $\vec{q}_L^3 = (1/2, -1/2, 1/2)$ and $\vec{q}_L^4 = (-1/2, -1/2, 1/2)$, in units $(2\pi/a)$. At $\vec{q} = \vec{q}_L^i$, $i = 1 - 4$, the eigenvalue spectrum of

the quadrupole matrix $v_{\Lambda\Lambda'}$ is the same and for simplicity we consider the arm \vec{q}_L^1 . Notice that at the L point there is a coupling between components of T_{2g} and E_g symmetry (see (A7) of Ref. 17). We write

$$v(\vec{q}_L^1) = \begin{bmatrix} v^{TT} & v^{TE} \\ v^{ET} & \hat{0} \end{bmatrix}, \quad (3.7)$$

where $\hat{0}$ stands for the 2×2 zero matrix, v^{TT} describes the 3×3 matrix between components of T_{2g} symmetry,

$$v^{TT}(\vec{q}_L^1) = -4 \begin{bmatrix} 0 & \beta & \beta \\ \beta & 0 & \beta \\ \beta & \beta & 0 \end{bmatrix}, \quad (3.8)$$

and v^{TE} stands for the 3×2 $T_{2g} - E_g$ coupling matrix,

$$v^{TE}(\vec{q}_L^1) = -4 \begin{bmatrix} \lambda & \nu \\ \lambda & -\nu \\ \mu & 0 \end{bmatrix}, \quad (3.9)$$

and $v^{ET} = (v^{TE})^\dagger$. The elements β , λ , μ and ν are obtained by integrals of the type (3.2a,b).

Diagonalizing the matrix v^{TT} we obtain the eigenvalues -8β , 4β , 4β and eigenvectors

$$S_{T_{2g}}^1(\vec{q}_L^1) = \frac{1}{\sqrt{3}}(S_{T_{2g}}^1(\vec{q}_L^1) + S_{T_{2g}}^2(\vec{q}_L^1) + S_{T_{2g}}^3(\vec{q}_L^1)), \quad (3.10a)$$

$$S_{T_{2g}}^2(\vec{q}_L^1) = \frac{1}{\sqrt{2}}(S_{T_{2g}}^1(\vec{q}_L^1) - S_{T_{2g}}^2(\vec{q}_L^1)), \quad (3.10b)$$

$$S_{T_{2g}}^3(\vec{q}_L^1) = \frac{1}{\sqrt{6}}(S_{T_{2g}}^1(\vec{q}_L^1) + S_{T_{2g}}^2(\vec{q}_L^1) - 2S_{T_{2g}}^3(\vec{q}_L^1)). \quad (3.10c)$$

In the basis $S_{T_{2g}}^1(\vec{q}_L^1)$, $S_{T_{2g}}^2(\vec{q}_L^1)$, $S_{E_g}^2(\vec{q}_L^1)$, $S_{T_{2g}}^3(\vec{q}_L^1)$, $S_{E_g}^1(\vec{q}_L^1)$ the matrix $v(\vec{q}_L^1)$ becomes block-diagonal,

$$v(\vec{q}_L^1) = -4 \begin{bmatrix} 2\beta & 0 & 0 & 0 & 0 \\ 0 & -\beta & \sqrt{2}\nu & 0 & 0 \\ 0 & \sqrt{2}\nu & 0 & 0 & 0 \\ 0 & 0 & 0 & -\beta & -\sqrt{\frac{3}{2}}\mu \\ 0 & 0 & 0 & -\sqrt{\frac{3}{2}}\mu & 0 \end{bmatrix}. \quad (3.11)$$

We find its eigenvalues, of which $\lambda_L^1 = -2(-\beta + \sqrt{\beta^2 + 8\nu^2})$ and $\lambda_L^2 = 2(\beta + \sqrt{\beta^2 + 8\nu^2})$ are double degenerate while $\lambda_L^3 = -8\beta$ is non degenerate. From numerical calculations we obtain $\beta = -33.54$ K, $\mu = -29.05$ K, $\lambda = 14.53$ K, $\nu = -25.16$ K and $\lambda_L^1 = -224.4$ K, $\lambda_L^2 = 90.3$ K and $\lambda_L^3 = 268.3$ K. These results are in agreement with the symmetry relations $2\nu = \sqrt{3}\mu$, $2\lambda = -\mu$, that hold for quadrupole-quadrupole Coulomb interactions on a fcc lattice. The lowest eigenvalue λ_L^1 has the eigenvectors

$$S^{(1)}(\vec{q}_L^1) = -0.5972(S_{T_{2g}}^1 - S_{T_{2g}}^2) + 0.5356 S_{E_g}^2, \quad (3.12a)$$

$$S^{(2)}(\vec{q}_L^1) = +0.3448(S_{T_{2g}}^1 + S_{T_{2g}}^2) - 0.6895 S_{T_{2g}}^3 + 0.5356 S_{E_g}^1, \quad (3.12b)$$

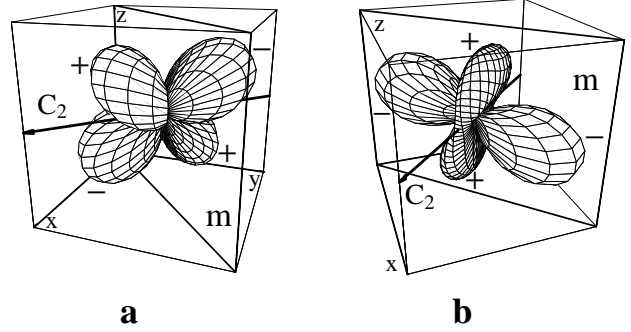


FIG. 1. Schematic pictures of two variants of quadrupole order parameter (quadrupole density); m is the mirror plane, C_2 is the rotation axis. a) $S^{(1)}$, Eq. (3.13a), which leads to $C2/c$, Eq. (3.15a); b) $S^{(2)}$, Eq. (3.13b), which leads to $C2/m$, Eq. (3.15b).

where we omit the arguments \vec{q}_L^1 on the right hand sides. In addition, we consider the corresponding functions in real space,

$$S^{(1)}(\Omega) = -0.5972(S_{T_{2g}}^1(\Omega) - S_{T_{2g}}^2(\Omega)) + 0.5356 S_{E_g}^2(\Omega), \quad (3.13a)$$

$$S^{(2)}(\Omega) = +0.3448(S_{T_{2g}}^1(\Omega) + S_{T_{2g}}^2(\Omega)) - 0.6895 S_{T_{2g}}^3(\Omega) + 0.5356 S_{E_g}^1(\Omega). \quad (3.13b)$$

These two functions are shown in Fig. 1a,b. We investigate their transformational properties in detail in Appendix A.

The quadrupolar densities which correspond to the functions $S^{(\alpha)}$, $\alpha = 1, 2$, are given by the expression

$$\rho_\alpha^F(\vec{n}) = \sum_{ij} |i\rangle_{\vec{n}} c_\alpha^F(ij) \langle j|_{\vec{n}} \quad (3.14a)$$

with

$$c_\alpha^F(ij) = \langle i|S^{(\alpha)}|j\rangle = \int d\Omega \langle i|\hat{n}\rangle S^{(\alpha)}(\hat{n}) \langle \hat{n}|j\rangle. \quad (3.14b)$$

(Compare with expressions (3.3), (3.4).)

The functions $S^{(\alpha)}$ belong to the two dimensional small representation E_g of the little group $\bar{3}m$ (D_{3d}) of $^*\vec{q}_L$ ($\hat{\tau}^5$ representation in Kovalev's notation³⁷). The irreducible representation of the space group $Fm\bar{3}m$ comprises eight such functions, with two functions from four arms of $^*\vec{q}_L$, that is, $S^{(1)}(\vec{q}_L^1)$, $S^{(2)}(\vec{q}_L^1)$; $S^{(1)}(\vec{q}_L^2)$, $S^{(2)}(\vec{q}_L^2)$; $S^{(1)}(\vec{q}_L^3)$, $S^{(2)}(\vec{q}_L^3)$ and $S^{(1)}(\vec{q}_L^4)$, $S^{(2)}(\vec{q}_L^4)$. In principle, there are many possibilities for condensations schemes at $^*\vec{q}_L$ involving one, two, three or four arms.^{38,39} Experimentally, reflections associated with all four components of the star $^*\vec{q}_L$ were clearly observed¹⁰ and had different intensities even in small applied magnetic fields. On this basis it was concluded in Ref. 10 that each arm of $^*\vec{q}_L$ is associated with a domain. We then limit our consideration

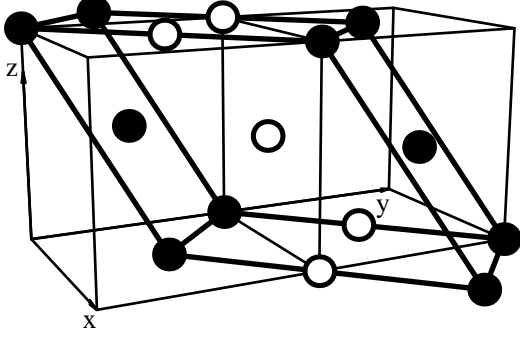


FIG. 2. Monoclinic unit cell in respect to cubic system of axes. Black and white circles refer to Tm sites where in case of $C2/c$ structure $\langle \rho_1^F \rangle$ (in case of $C2/m$ $\langle \rho_2^F \rangle$) is taken with the sign + for black and - for white circles.

to the case where a single arm, say \vec{q}_L^1 , is involved in the symmetry lowering which occurs due to the quadrupolar ordering. In such case the following two condensation schemes are possible³⁹:

$$Fm\bar{3}m : L_3^+ [\langle \rho_1^F(\vec{q}_L^1) \rangle = \sqrt{N}\rho_1] \rightarrow C2/c (Z = 2), \quad (3.15a)$$

$$Fm\bar{3}m : L_3^+ [\langle \rho_2^F(\vec{q}_L^1) \rangle = \sqrt{N}\rho_2] \rightarrow C2/m (Z = 2). \quad (3.15b)$$

Here $\rho_\alpha^F(\vec{q})$ stands for the Fourier transform of $\rho_\alpha^F(\vec{n})$, $\langle \dots \rangle$ denotes a thermal average and ρ_α are the order parameter amplitudes. Correspondingly, in real space we obtain

$$\langle \rho_\alpha^F(\vec{n}) \rangle = \rho_\alpha \cos(\vec{q}_L^1 \cdot \vec{X}(\vec{n})), \quad \alpha = 1, 2. \quad (3.16)$$

Both structures are monoclinic, with the mirror plane $[1\bar{1}0]$, see also Figs. 1a,b. As follows from Eq. (3.16) $\langle \rho_1^F(\vec{n}) \rangle$ and $\langle \rho_2^F(\vec{n}) \rangle$ change from $+\rho_1$ to $-\rho_1$ and from $+\rho_2$ to $-\rho_2$, respectively, along the $[110]$ direction. The resulting pattern as well as the monoclinic unit cell are shown in Fig. 2. We speak of an antiferro-quadrupolar order. At \vec{q}_L^1 there are still three variants of condensations of the type (3.15a) and three of the type (3.15b). For example, we consider the condensation in $C2/c$, Eq. (3.15a). The three variants involve condensations of quadrupolar functions $S'^{(1)}$ which are obtained from $S^{(1)}$ through rotations by the angle 0, $2\pi/3$ and $4\pi/3$ about the cubic axis $[111]$. Notice that this functions can be expressed in terms of a linear combinations of $S^{(1)}$, $S^{(2)}$ since they form a basis of the little group $\bar{3}m (D_{3d})$ of \vec{q}_L^1 . Otherwise, the consideration is the same as for $S^{(1)}$, $S^{(2)}$. The corresponding monoclinic unit cells are obtained from that in Fig. 2 through the same rotations by the angle 0, $2\pi/3$ and $4\pi/3$. For example, for the rotation by $2\pi/3$ the basal (xy) plane (see Fig. 2) transforms to (yz) while the monoclinic mirror plane

$[1\bar{1}0]$ becomes $[01\bar{1}]$. These three variants correspond to the so-called ‘‘S domains’’ which have been observed in neutron diffraction experiments¹⁰ for a given arm of $^*\vec{q}_L$. However, the total number of domains for the condensation to $C2/c$ is twelve. The same holds for the second condensation scheme, Eq. (3.15b), to the $C2/m$ monoclinic structure. We conclude that on the basis of data from neutron diffraction¹⁰ on TmTe it is not possible to deduce which of the two ordered structures actually occurs in TmTe. Both structures are monoclinic and lead to the domain structure observed in experiment.¹⁰ On the other hand, from our theoretical analysis of coupling matrices we cannot rule out one structure in favor of the other. In the next section we show that the two types of quadrupolar ordering can be distinguished by lattice displacements which accompany the transition. The condensation scheme (3.15a) corresponds to that given by Eq. (3.10a) of Ref. 40, where two complex basis functions of the $\hat{\tau}^5$ irreducible representation are used.

In the following we study the thermodynamics of the quadrupolar phase transitions. Taking into account the first condensation scheme, Eq. (3.15a), we obtain for the quadrupole coupling at a site \vec{n}_1 for one sublattice ($\{\vec{n}_1\}$)

$$U_{QQ}^{ff}(\vec{n}_1) = \lambda_L^1 \rho_1 \rho_1^F(\vec{n}_1), \quad (3.17)$$

where ρ_1 is the order parameter amplitude and where $\rho_1^F(\vec{n}_1)$ is the quadrupolar density operator. The mean field Hamiltonian reads

$$H^{MF}(\vec{n}_1) = U_{QQ}^{ff}(\vec{n}_1) + V_0^f(\vec{n}_1), \quad (3.18)$$

where V_0^f , Eq. (2.2), describes the crystal field and the spin-orbit coupling. Starting with H^{MF} and using methods which have been developed for molecular crystals⁴¹, we obtain the following approximate expression for the Landau free energy:

$$\mathcal{F}/N = \mathcal{F}_0/N + A\rho_1^2 + B\rho_1^4. \quad (3.19)$$

Here \mathcal{F}_0 is the free energy in the disordered phase

$$\mathcal{F}_0/N = -T \ln Z_0, \quad (3.20)$$

where

$$Z_0 = \sum_{i=1}^{14} e^{-\varepsilon_i/T} \quad (3.21)$$

is the sum of states and ε_i are the crystal field energy levels. The expansion coefficients in Eq. (3.19) are

$$A = \frac{1}{2} \left(\frac{T}{x^{(2)}} + \lambda_L^1 \right), \quad (3.22a)$$

$$B = \frac{T}{24[x^{(2)}]^2} \left(3 - \frac{x^{(4)}}{[x^{(2)}]^2} \right), \quad (3.22b)$$

where

TABLE III. Calculated parameters of the Landau free energy expansion, see text for details.

$x^{(2)}$	$x^{(4)}$	B/T	k
0.0219	0.000768	121.5	0.188

$$x^{(2)} = \sum_{ij} c_1^F(ij) c_1^F(ji) e^{-\varepsilon_i/T} / Z_0, \quad (3.23a)$$

$$x^{(4)} = \sum_{ijhl} c_1^F(ij) c_1^F(jh) c_1^F(hl) c_1^F(li) e^{-\varepsilon_i/T} / Z_0. \quad (3.23b)$$

The calculation of $x^{(2)}$ and $x^{(4)}$ requires the knowledge of the crystal field. Using the values of ε_i from Table II and the corresponding calculated eigenvectors, we obtain the results quoted in Table III. Since there is no third order cubic invariant in expression (3.19) and since $B > 0$, the phase transition is of second order, with the transition temperature given by

$$T_c = x^{(2)} |\lambda_L^1| \quad (3.24)$$

and the order parameter amplitude given at $T < T_c$ by

$$\rho_1(T) = \pm \sqrt{-\frac{A}{2B}} = \pm \sqrt{k \frac{T_c - T}{T}}, \quad (3.25)$$

where

$$k = \frac{12(x^{(2)})^3}{3(x^{(2)})^2 - x^{(4)}}. \quad (3.26)$$

With $\lambda_L^1 = -224.4$ K we find $T_c = 4.9$. This value is more than twice the experimental temperature $T_Q = 1.8$ K. We ascribe the origin of the discrepancy to the screening effect of conduction electrons from Tm and Te sites and from the interstitial region. The question may arise why in case of cerium the polarization of conduction electrons leads to an increase of transition temperature¹⁹, while in case of TmTe it has the opposite effect. We recall that in Ce quadrupoles constructed from conduction electrons are in close contact and their ordering greatly reduces the repulsion between conduction electrons. In TmTe 4f holes and conduction electrons around Tm sites are at larger distances and the polarization of conduction electrons merely reduces the resulting effective quadrupolar value.

Finally we mention that with Eqs. (3.17)-(3.24) we readily obtain the corresponding expressions for the second condensation scheme (3.15b) by replacing the index 1 in ρ_1 and $c_1(ij)$ by the index 2. The numerical values of $x^{(2)}$, $x^{(4)}$, B and T_c remain the same and therefore no distinction between $C2/c$ and $C2/m$ can be made at this point.

IV. LATTICE DISTORTIONS

The quadrupolar ordering and symmetry lowering is accompanied by a distortion of the cubic lattice. Such

effects are known to occur in molecular crystals (see for a review Ref. 42) and our present treatment^{18,19} was inspired by the theory of orientational order in molecular solids.^{43,42}

We consider the Tm atoms located on a non rigid fcc lattice and denote the lattice displacement of the Tm nucleus at site \vec{n} by $\vec{u}(\vec{n})$. For the 4f hole coordinates we have

$$\vec{R}(\vec{n}) = \vec{X}(\vec{n}) + \vec{r}(\vec{n}) + \vec{u}(\vec{n}), \quad (4.1)$$

where $\vec{X}(\vec{n})$ stands for equilibrium nuclear position. We expand the intersite potential (3.1) in terms of atomic lattice displacements. The first order correction to the potential reads

$$U_{QQT}^{(\alpha)} = \frac{1}{2} \sum'_{\vec{n}\vec{n}'} \sum_{\nu} v_{\nu}^{(\alpha)}(\vec{n} - \vec{n}'; r, r') \times S^{(\alpha)}(\hat{n}) S^{(\alpha)}(\hat{n}') [u_{\nu}(\vec{n}) - u_{\nu}(\vec{n}')], \quad (4.2)$$

where

$$v_{\nu}^{(\alpha)}(\vec{n} - \vec{n}'; r, r') = \int d\Omega(\vec{n}) \int d\Omega(\vec{n}') S^{(\alpha)}(\hat{n}) S^{(\alpha)}(\hat{n}') \times \frac{\partial}{\partial X_{\nu}(\vec{n})} \frac{1}{|\vec{R}(\vec{n}) - \vec{R}'(\vec{n}')|} \Big|_{\vec{u}=0}. \quad (4.3)$$

Here the index α ($\alpha = 1, 2$) corresponds to the two variants of antiferro- quadrupole ordering, Eqs. (3.15a,b). We recall that $\vec{n} - \vec{n}'$ stands for $\vec{X}(\vec{n} - \vec{n}') \equiv \vec{X}(\vec{\kappa})$. We take the average over the radial dependence of the 4f hole:

$$v_{\nu}^{(\alpha)}(\vec{\kappa}) = \int dr r^2 \int dr' r'^2 \mathcal{R}_f^2(r) \mathcal{R}_f^2(r') v_{\nu}^{(\alpha)}(\vec{\kappa}; r, r'). \quad (4.4)$$

One has the symmetry relation

$$v_{\nu}^{(\alpha)}(\vec{\kappa}) = -v_{\nu}^{(\alpha)}(-\vec{\kappa}) \quad (4.5)$$

on the fcc lattice. In the following $\vec{\kappa}$ labels the twelve nearest neighboring Tm sites around a Tm ion taken as origin. Proceeding as in Ref. 18 we rewrite the expression (4.2) as an operator in the space of the 4f hole:

$$U_{QQT}^{(\alpha)} = \frac{1}{2} \sum'_{\vec{n}\vec{n}'} \sum_{\nu} v_{\nu}^{(\alpha)}(\vec{n} - \vec{n}') \times \rho_{\alpha}^F(\vec{n}) \rho_{\alpha}^F(\vec{n}') [u_{\nu}(\vec{n}) - u_{\nu}(\vec{n}')], \quad (4.6)$$

where $\rho_{\alpha}^F(\vec{n})$ is defined by expressions (3.14a,b). Transforming to Fourier space we find

$$U_{QQT}^{(\alpha)} = i \sum_{\vec{k}} \sum_{\vec{p}} v_{\nu}^{(\alpha)}(\vec{k}, \vec{p}) \rho_{\alpha}^F(-\vec{p} - \vec{q}) \rho_{\alpha}^F(\vec{p}) u_{\nu}(\vec{k}), \quad (4.7)$$

where

$$v'_\nu(\alpha)(\vec{k}, \vec{p}) = (Nm)^{-1/2} \sum_{\vec{\kappa}} v'_\nu(\alpha)(\vec{\kappa}) \times \cos[(\vec{p} + \frac{\vec{k}}{2}) \cdot \vec{X}(\vec{\kappa})] \sin[\frac{\vec{k} \cdot \vec{X}(\vec{\kappa})}{2}]. \quad (4.8)$$

In order to obtain the free energy contribution from $U_{QQT}^{(\alpha)}$, we take the long wavelength limit $\vec{k} \rightarrow 0$ and retain only linear terms in \vec{k} . We then consider \vec{p} near \vec{q}_L^1 and apply the condensation schemes (3.15a,b). Finally we replace the displacements $u_\nu(\vec{k})$ by their instantaneous thermal expectation values $\langle u_\nu(\vec{k}) \rangle$. After some algebra we obtain

$$F_{QQT}^{(\alpha)} = \frac{N}{2\sqrt{Nm}} (\rho_\alpha)^2 \times \sum_{\nu=x,y,z} [ik_x \Lambda_{x\nu}^{(\alpha)} + ik_y \Lambda_{y\nu}^{(\alpha)} + ik_z \Lambda_{z\nu}^{(\alpha)}] \langle u_\nu(\vec{k}) \rangle, \quad (4.9)$$

where ρ_α is the order parameter amplitude. In (4.9) we have defined

$$\Lambda_{x\nu}^{(\alpha)} = -a[v'_\nu(\alpha)(3) + v'_\nu(\alpha)(2) + v'_\nu(\alpha)(6) + v'_\nu(\alpha)(5)], \quad (4.10a)$$

$$\Lambda_{y\nu}^{(\alpha)} = -a[v'_\nu(\alpha)(1) + v'_\nu(\alpha)(3) + v'_\nu(\alpha)(4) - v'_\nu(\alpha)(6)], \quad (4.10b)$$

$$\Lambda_{z\nu}^{(\alpha)} = -a[v'_\nu(\alpha)(1) + v'_\nu(\alpha)(2) - v'_\nu(\alpha)(4) - v'_\nu(\alpha)(5)]. \quad (4.10c)$$

Here the arguments $\vec{\kappa} = 1 - 6$ of $v'_\nu(\alpha)$ stand for $\vec{X}(\vec{\kappa})$, with $\vec{X}(1) = (0, 1, 1)$, $\vec{X}(2) = (1, 0, 1)$, $\vec{X}(3) = (1, 1, 0)$, $\vec{X}(4) = (0, -1, 1)$, $\vec{X}(5) = (-1, 0, 1)$, $\vec{X}(6) = (-1, 1, 0)$ in units $a/2$, where a is the cubic lattice constant. Introducing the homogeneous strains

$$\lim_{\vec{k} \rightarrow 0} ik_\mu \langle u_\nu(\vec{k}) \rangle = \sqrt{mN} \epsilon_{\mu\nu}, \quad \nu = x, y, z, \quad (4.11)$$

we obtain

$$F_{QQT}^{(\alpha)}[\epsilon, \rho]/N = \rho_\alpha^2 [\Lambda_{xx}^{(\alpha)} (\epsilon_{xx} + \epsilon_{yy}) + \Lambda_{zz}^{(\alpha)} \epsilon_{zz} + 2\Lambda_{xy}^{(\alpha)} \epsilon_{xy} + 2\Lambda_{xz}^{(\alpha)} (\epsilon_{xz} + \epsilon_{yz})]. \quad (4.12)$$

(From the symmetry of the order parameters it follows that $\Lambda_{xx}^{(\alpha)} = \Lambda_{yy}^{(\alpha)}$ and $\Lambda_{xz}^{(\alpha)} = \Lambda_{yz}^{(\alpha)}$.) It is convenient to work in the system of axes which reflects the monoclinic symmetry, Fig. 2. We therefore consider the coordinate system $x'y'z'$, where x' axis corresponds to $[1\bar{1}0]$, y' - to $[110]$ and z' to $[001]$ directions of the cubic system. Notice that the new axes are obtained by the clockwise rotation about the z axis by $\pi/4$. Since $\Lambda_{\mu\nu}$ ($\mu, \nu = x, y, z$) is a tensor of the second rank, we write $F_{QQT}^{(\alpha)}[\epsilon, \rho]$ in the new coordinate system as

$$F_{QQT}^{(\alpha)}[\epsilon', \rho]/N = \rho_\alpha^2 \times [\Lambda'_{xx}(\alpha) \epsilon'_{xx} + \Lambda'_{yy}(\alpha) \epsilon'_{yy} + \Lambda'_{zz}(\alpha) \epsilon'_{zz} + 2\Lambda'_{yz}(\alpha) \epsilon'_{yz}]. \quad (4.13)$$

TABLE IV. Calculated parameters $\Lambda'_{\mu\nu}(1)$ and homogeneous strains $\epsilon'_{\mu\nu}$ for the quadrupolar ordering $Fm\bar{3}m \rightarrow C2/c$; ρ_1 is the order parameter amplitude.

$\mu \nu$	xx	yy	zz	yz
$\Lambda'_{\mu\nu}(1)$	155.7 K	94.2 K	311.1 K	243.6 K
$[\epsilon'_{\mu\nu}/(\rho_1)^2] \times 10^4$	-2.08	+1.95	-4.66	-16.0

In the transformed coordinate system the elastic term of the free energy reads

$$F_{TT}[\epsilon']/(V_c N) = \frac{1}{2} c_5 (\epsilon'_{xx}{}^2 + \epsilon'_{yy}{}^2) + \frac{1}{2} c_{11} \epsilon'_{zz}{}^2 + c_{12} (\epsilon'_{xx} + \epsilon'_{yy}) \epsilon'_{zz} + c_6 \epsilon'_{xx} \epsilon'_{yy} + (c_{11} - c_{12}) \epsilon'_{xy}{}^2 + 2c_{44} \epsilon'_{yz}{}^2, \quad (4.14)$$

where we have introduced the notations $c_5 = (c_{11} + c_{12})/2 + c_{44}$, $c_6 = (c_{11} + c_{12})/2 - c_{44}$ and c_{11} , c_{12} , c_{44} are the cubic elastic constants. Minimizing $F_{QQT} + F_{TT}$ with respect to the strains $\epsilon'_{\mu\nu}$ for a given configuration with a fixed expectation value ρ_α we obtain:

$$\epsilon'_{xx} = -\frac{\rho_\alpha^2}{2c_{44}\Delta V_c} [\Lambda'_{xx}(\alpha) (c_{11}c_5 - c_{12}^2) - \Lambda'_{yy}(\alpha) (c_{11}c_6 - c_{12}^2) - 2\Lambda'_{zz}(\alpha) c_{12}c_{44}], \quad (4.15a)$$

$$\epsilon'_{yy} = -\frac{\rho_\alpha^2}{2c_{44}\Delta V_c} [\Lambda'_{yy}(\alpha) (c_{11}c_5 - c_{12}^2) - \Lambda'_{xx}(\alpha) (c_{11}c_6 - c_{12}^2) - 2\Lambda'_{zz}(\alpha) c_{12}c_{44}], \quad (4.15b)$$

$$\epsilon'_{zz} = -\frac{\rho_\alpha^2}{\Delta V_c} [\Lambda'_{zz}(\alpha) (c_{11} + c_{12}) - c_{12} (\Lambda'_{xx}(\alpha) + \Lambda'_{yy}(\alpha))], \quad (4.15c)$$

$$\epsilon'_{yz} = -\frac{\rho_\alpha^2}{2c_{44}V_c} \Lambda'_{yz}(\alpha), \quad (4.15d)$$

where $\Delta = -2c_{12}^2 + c_{11}(c_{11} + c_{12})$. The shear distortion ϵ'_{yz} implies that in the monoclinic phases the angle between the axes y'_m and z'_m attached to the crystal deviates from $\pi/2$ by $\alpha \approx 2\epsilon'_{yz}$.

We now present numerical results for the quadrupole order in the $C2/c$ structure. In the monoclinic system of axes ($x'y'z'$) the calculated values are quoted in Table IV. (The shear angle $\alpha \approx -32 \cdot 10^{-4} \rho_1^2$.) For calculations of $\epsilon'_{\mu\nu}$ we took the elastic constants $c_{11} = 10285$, $c_{12} = 3969$ and $c_{44} = 1188$ in units $\text{K}/\text{\AA}^3$ from Ref. 9. Returning now to the original cubic system of axes (x, y, z) we find

$$\epsilon_{xx} = \epsilon_{yy} = -0.07 \cdot 10^{-4} \rho_1^2, \quad \epsilon_{zz} = -4.66 \cdot 10^{-4} \rho_1^2, \\ \epsilon_{xy} = +2.02 \cdot 10^{-4} \rho_1^2, \quad \epsilon_{xz} = \epsilon_{yz} = -11.3 \cdot 10^{-4} \rho_1^2. \quad (4.16)$$

For the condensation scheme (3.15b) to the $C2/m$ quadrupole structure the calculated values are quoted in Table V (the shear angle $\alpha = -6.84 \cdot 10^{-4} \rho_2^2$). In the initial cubic system of axes we find

TABLE V. Calculated parameters $\Lambda'_{\mu\nu}{}^{(2)}$ and homogeneous strains $\epsilon'_{\mu\nu}$ for the quadrupolar ordering $Fm\bar{3}m \rightarrow C2/m$; ρ_2 is the order parameter amplitude.

$\mu \nu$	xx	yy	zz	yz
$\Lambda'_{\mu\nu}{}^{(2)}$	9.2 K	488.9 K	63.0 K	52.3 K
$[\epsilon'_{\mu\nu}/(\rho_2)^2] \times 10^4$	+12.61	-18.87	+1.46	-3.42

$$\begin{aligned} \epsilon_{xx} = \epsilon_{yy} &= -3.13 \cdot 10^{-4} \rho_2^2, & \epsilon_{zz} &= +1.46 \cdot 10^{-4} \rho_2^2, \\ \epsilon_{xy} &= -15.74 \cdot 10^{-4} \rho_2^2, & \epsilon_{xz} = \epsilon_{yz} &= -2.42 \cdot 10^{-4} \rho_2^2. \end{aligned} \quad (4.17)$$

We conclude that the two possibilities of quadrupole order lead to completely different displacements in the monoclinic phase.

V. CONCLUSIONS

We present a microscopic model of quadrupole order in TmTe. For a $4f$ hole above T_Q we have obtained the sequence $\Gamma_7 - \Gamma_8 - \Gamma_6$ of the crystal electric field (CEF) energy spectrum with Γ_7 as ground state which is in agreement with results from Mössbauer spectroscopy²³ and ultrasonic velocity measurements.²⁴ The splitting of CEF levels is found to be small if only contributions from six Te nearest neighbors of a Tm site are taken into account.

We have considered quadrupolar interactions between $4f$ holes located on Tm sites. On the basis of neutron diffraction experiments¹⁰ indicating that a single arm of *q_L is responsible for the quadrupole structure, we have studied the quadrupole interactions at the L point of the BZ. We have found that the quadrupole coupling between $4f$ holes becomes attractive at the L point thus driving a structural phase transition with concomitant lowering of the crystal symmetry. Starting with the mean-field Hamiltonian we have derived the Landau free energy, calculated the transition temperature and found $T_c = 4.9$ K. The overestimation of the transition temperature is ascribed to a screening effect from conduction electrons which has not been considered in the present work. The structure of TmTe below T_Q is monoclinic (Fig. 2) but there are still two possibilities for the quadrupole order parameter. These quadrupole order parameters are expressed in real space in terms of T_{2g} and E_g components and visualized in Fig. 1. The condensation of ρ_1^F , Eq. (3.15a), leads to the $C2/c$ structure while the condensation of ρ_2^F , Eq. (3.15b), leads to the $C2/m$. Although both structures are monoclinic their symmetries are different. Both of them result in the domain variants which have been observed experimentally. We conclude that on the basis of the present experimental data and our theoretical studies it is impossible to determine unambiguously the actual quadrupole order in TmTe. We have shown that such discrimination could be done in respect to lattice distortions which develop below T_Q .

Starting from the quadrupole-quadrupole interactions on a deformable lattice, we have derived the couplings of the quadrupoles with the atomic lattice displacements. We have calculated the corresponding lattice distortions and suggest experiments which can be decisive in determining which quadrupole order is realized in TmTe.

ACKNOWLEDGMENTS

We thank J.M. Mignot and A. Gukasov for useful discussions. This work has been financially supported by the Fonds voor Wetenschappelijk Onderzoek, Vlaanderen.

APPENDIX A:

Here we investigate transformational properties of functions $S^{(1)}(\Omega)$ and $S^{(2)}(\Omega)$, Eqs. (3.13a,b) (see Fig. 1). Below we omit the argument Ω of the functions. We recall that the functions $S_{T_{2g}}^1$, $S_{T_{2g}}^2$ and $S_{T_{2g}}^3$ are proportional to the Cartesian components yz , zx and xy , respectively. Therefore, for the reflection m through the plane $[1\bar{1}0]$

$$m(S_{T_{2g}}^1 - S_{T_{2g}}^2) = -(S_{T_{2g}}^1 - S_{T_{2g}}^2), \quad (A1)$$

$$m(S_{T_{2g}}^1 + S_{T_{2g}}^2) = +(S_{T_{2g}}^1 + S_{T_{2g}}^2), \quad (A2)$$

while for the rotation C_2 by π about the axis $[1\bar{1}0]$

$$C_2(S_{T_{2g}}^1 - S_{T_{2g}}^2) = -(S_{T_{2g}}^1 - S_{T_{2g}}^2), \quad (A3)$$

$$C_2(S_{T_{2g}}^1 + S_{T_{2g}}^2) = +(S_{T_{2g}}^1 + S_{T_{2g}}^2). \quad (A4)$$

Therefore,

$$mS^{(1)} = -S^{(1)}, \quad (A5)$$

$$C_2S^{(1)} = -S^{(1)}, \quad (A6)$$

while

$$mS^{(2)} = S^{(2)}, \quad (A7)$$

$$C_2S^{(2)} = S^{(2)}. \quad (A8)$$

* Also: Institute of Physical Chemistry of RAS, Leninskii prospect 31, Moscow, 117915, Russia.

¹ P. Wachter, in *Handbook on the Physics and Chemistry of Rare Earths*, v. 19, eds. K.A. Gschneidner, Jr., L. Eyring, G.H. Lander and G.R. Choppin (Elsevier Science, Amsterdam, 1994), p. 177.

² R. Suryanarayanan, G. Güntherodt, J.L. Freeouf, F. Holtzberg, Phys. Rev. B **12**, 4215 (1975).

³ Y. Lassailly, C. Vettier, F. Holtzberg, A. Benoit, J. Flouquet, Solid State Commun. **52**, 717 (1984).

- ⁴ T. Matsumura, T. Kosaka, J. Tang, T. Matsumoto, H. Takahashi, N. Mōri, T. Suzuki, Phys. Rev. Lett. **78**, 1138 (1997).
- ⁵ P. Link, I.N. Goncharenko, J.M. Mignot, T. Matsumura, T. Suzuki, Phys. Rev. Lett. **80**, 173 (1998).
- ⁶ S. Heathman, T. Le Bihan, S. Darracq, C. Abraham, D.J.A. De Ridder, U. Benedict, K. Mattenberger, O. Vogt, J. Alloys Compd. **230**, 89 (1995).
- ⁷ J. Tang, T. Kosaka, T. Matsumura, T. Matsumoto, N. Mori, T. Suzuki, Solid State Commun. **100**, 571 (1996).
- ⁸ T. Matsumura, Y. Haga, Y. Nemoto, S. Nakamura, T. Goto, T. Suzuki, Physica B **206-207**, 380 (1995); T. Matsumura, S. Nakamura, T. Goto, H. Shida, T. Suzuki, Physica B **223-224**, 385 (1996).
- ⁹ T. Matsumura, S. Nakamura, T. Goto, H. Amitsuka, K. Matsuhira, T. Sakakibara, T. Suzuki, J. Phys. Soc. Jpn **67**, 612 (1998).
- ¹⁰ P. Link, A. Gukasov, J.M. Mignot, T. Matsumura, T. Suzuki, Phys. Rev. Lett. **80**, 4779 (1998).
- ¹¹ J.-M. Mignot, P. Link, A. Gukasov, I.N. Goncharenko, T. Matsumura, T. Suzuki, Physica B **281-282**, 470 (2000).
- ¹² P. Link, T. Matsumura, A. Gukasov, J.-M. Mignot, T. Suzuki, Physica B **281-282**, 569 (2000).
- ¹³ J.-M. Mignot, I.N. Goncharenko, P. Link, T. Matsumura, A. Gukasov, T. Suzuki, Physica B **276**, 756 (2000).
- ¹⁴ see for a review P. Morin and D. Schmitt, in *Ferromagnetic Materials*, K.H.J. Buschow and E.P. Wohlfarth Eds. (North-Holland, Amsterdam, 1990), v. 5, p. 1.
- ¹⁵ R. Shiina, H. Shiba, O. Sakai, J. Phys. Soc. Jpn **68**, 2105 (1999).
- ¹⁶ R. Shiina, H. Shiba, O. Sakai, J. Phys. Soc. Jpn **68**, 2390 (1999).
- ¹⁷ K.H. Michel, J.R.D. Copley, Z. Phys. B Cond. Matter **103**, 369 (1997).
- ¹⁸ A.V. Nikolaev and K.H. Michel, Eur. Phys. J. B **9**, 619 (1999); **17**, 363 (2000).
- ¹⁹ A.V. Nikolaev and K.H. Michel, Eur. Phys. J. B, **17**, 15 (2000).
- ²⁰ E. Bucher, K. Andres, F.J. di Salvo, J.P. Maita, A.C. Gosard, A.S. Cooper, G.W. Hull, Jr., Phys. Rev. B **11**, 500 (1975).
- ²¹ H.R. Ott and B. Lüthi, Z. Phys. B **28**, 141 (1977).
- ²² E. Clementyev, R. Köhler, M. Braden, J.M. Mignot, C. Vettier, T. Matsumura, T. Suzuki, Physica B **230-232**, 735 (1997).
- ²³ B.B. Triplett, Y. Mahmud, N.S. Dixon, S.S. Hanna, F. Holtzberg, Phys. Lett. A **67**, 151 (1978).
- ²⁴ T. Kasuya, J. Phys. Soc. Jpn. **63**, 3936 (1994).
- ²⁵ K.R. Lea, M.J.M. Leask, W.P. Wolf, J. Phys. Chem. Solids **23**, 1381 (1962).
- ²⁶ K.W.H. Stevens, Proc. Phys. Soc. **A65**, 209 (1952); M.T. Hutchings, in *Solid State Physics: Advances in Research and Applications*, Eds. F. Seitz and D. Turnbull, v. 16, (Academic Press, New York, 1964), p. 227.
- ²⁷ D.J. Newman, Adv. Phys. **20**, 197 (1971).
- ²⁸ D.J. Newman, J. Phys. F: Met. Phys. **13**, 1511 (1983).
- ²⁹ M.R. Norman, H.J.F. Jansen, Phys. Rev. B **37**, 10050 (1988).
- ³⁰ The code has been written and tested in the Institute of Physical Chemistry of RAS, G.V. Ionova, A.V. Nikolaev, Phys. Stat. Sol. B **162**, 451 (1990).
- ³¹ D.J. Singh, *Planewaves, Pseudopotentials and the LAPW method*, (Kluwer, Boston, 1994).
- ³² C. J. Bradley and A. P. Cracknell, *The Mathematical Theory of Symmetry in Solids*, (Clarendon, Oxford, 1972).
- ³³ The influence of the interstitial electron charge density on CEF calculation will be discussed in a separate paper.
- ³⁴ H. Yasuda and T. Yamamoto, Prog. Theor. Phys. **45**, 1458 (1971); R. Heid, Phys. Rev. B **47**, 15912 (1993).
- ³⁵ S.E. Barnes, K. Baberschke, M. Hardiman, Phys. Rev. B **18**, 2409 (1978).
- ³⁶ O.K. Andersen, Phys. Rev. B **12**, 3060 (1975).
- ³⁷ O.V. Kovalev, *Irreducible Representations of the Space Groups*, (Gordon and Breach, New York, 1965).
- ³⁸ P. Launois, private communication.
- ³⁹ H.T. Stokes and D.M. Hatch, *Isotropy subgroups of the 230 crystallographic space groups*, (World Scientific, Singapore, 1988).
- ⁴⁰ K. Parlinski, Z. Phys. B - Condensed Matter **56**, 51 (1984).
- ⁴¹ K.H. Michel and K. Parlinski, Phys. Rev. B **31**, 1823 (1985).
- ⁴² R. M. Lynden-Bell and K. H. Michel, Rev. Mod. Phys. **66**, 721 (1994).
- ⁴³ D. Lamoen and K.H. Michel, Phys. Rev. B **48**, 807 (1993).